(Received 21 January 2025, Accepted 8 July 2025, Scheduled 6 August 2025)

X/Ku-Band Antenna with Integrated Back Cavity for Directional Radiation

Jiawei Wang[1], Tao Tang[1], Thamer S. Almoneef[2,*], and Maged A. Aldhaeebi[2]

[1] College of Electronic and Information, Southwest Minzu University, Chengdu 610225, Sichuan, China
[2] Department of Electrical Engineering, Prince Sattam Bin Abdulaziz University, Al-Kharj 11942, Saudi Arabia

ABSTRACT: This paper presents a dual-band antenna design for X/Ku bands, featuring asymmetrical feed ports, slot-loaded radiating patches, and a reconfigured defect ground structure (DGS) integrated with a back air cavity to achieve 32.11% reduced patch area and directional radiation. By coplanar waveguide (CPW) feeding and vertical interconnect accesses (VIAs) connecting all metal layers, the antenna miniaturizes via extended surface current paths and broadens bandwidth via DGS. Simulation and measurement show operating bands of 8.30–12.29 GHz (38.75% fractional bandwidth) and 12.91–14.21 GHz (9.58%), with measured gains aligning well with simulations. Compared to traditional dual-band designs, this work reduces physical size by over 30% while maintaining high gain, making it suitable for compact satellite communication, radar, and microwave energy systems.

1. INTRODUCTION

In the advancing landscape of wireless communication, antennas remain indispensable, bridging the gap between electronic signals and the transmission of information through space. The advent of dual-band antennas, particularly those operating in the X and Ku frequency bands, has significantly expanded the horizons of wireless communication, radar, and satellite systems [1, 2]. These bands are highly sought after due to their ability to support high-data-rate transmissions and long-range communications [3]. However, dual-band antennas for X and Ku bands often rely on complex multi-resonator designs or metamaterial-enhanced backside structures to achieve broad bandwidth performance [4–6].

As the demand for compact and high-performance antennas escalates, coplanar waveguide (CPW) structure has emerged as a promising candidate [7–9]. Its planar configuration facilitates the integration with monolithic microwave integrated circuits (MMICs), enhancing the overall system's compactness and efficiency. Furthermore, the incorporation of a back cavity in the antenna design has been recognized for its potential to enhance radiation performance, including gain and directivity, without a proportional increase in the antenna's physical size [10, 11]. However, the introduction of an additional or independent back cavity, while boosting radiation performance, often leads to an increased antenna volume, negating the low-profile advantage typically associated with CPW designs [12, 13].

Directional antennas offer several advantages over their omnidirectional counterparts, including reduced interference, enhanced spatial frequency reuse, extended transmission ranges, and increased network capacity. These benefits have facilitated a variety of innovative outdoor and indoor applications, as extensively documented in contemporary research [14, 15]. In the design of directional antennas, the incorporation of reflectors is a common approach to enhance gain and directivity [16]. However, the addition of reflectors can hinder miniaturization efforts. Recently, metamaterials have emerged as an alternative for reflector elements, offering the capability to manipulate directionality. Despite their potential, the integration of metamaterials introduces complexity in the antenna design process [17]. However, existing X/Ku dual-band antennas often rely on complex multi-resonator structures or metamaterial-enhanced backsides, leading to large size and limited control over radiation directionality, which restricts their use in compact, high-performance systems.

In this work, we present an innovative dual-band antenna design that achieves miniaturization by creating slots on the radiating patch and positioning the feed port off center on one side, effectively increasing the equivalent path length of the patch surface current. The incorporation of a DGS broadens the antenna's operation bandwidth. Behind the patch, we place a substrate with a strategically cut-out middle part, and the cut-out bottom is covered by a metal layer to form a back-air cavity. To facilitate integration with the back cavity, the DGS was reconfigured to be coplanar with the patch. The back cavity is integrated with all metal layers and the antenna through vertical interconnect accesses (VIAs), which are strategically placed on both sides of the feed line and the lower side near the patch. The back cavity not only introduces a new resonance and expands part of the frequency band, but also utilizes the metal ground behind the air cavity as a reflector, steering the radiation pattern into a unidirectional forward radiation mode.

This configuration effectively supports operation in both the X-band and Ku-band. It also shows potential in directional electromagnetic energy transmission, microwave wire-

* Corresponding author: Thamer S. Almoneef (t.almoneef@psau.edu.sa).

TABLE 1. Detailed dimension parameters (unit: mm).

Parameter	$L1$	$L2$	$L3$	$L4$	$L5$	$L6$	$W1$	$W2$	$W3$	$W4$	$g1$	$g2$
Value	32	29	20.5	4.5	13	8	32	22	18	4	0.27	3.928

less charging, microwave energy harvesting, satellite communication, and radar systems.

2. CONFIGURATION AND RESULTS

The antenna configuration is shown in Fig. 1, where (a) is the front view of the antenna, highlighting the asymmetric radiant patch fed laterally by the coplanar waveguide structure; (b) is the upper surface of the air cavity; (c) is the bottom metal ground; and (d) is the overall cross-section which more intuitively shows the structure of the entire antenna. FR4 with a relative permittivity of 4.4 is used as the antenna design substrate. Among them, the thickness of the substrate where the patch is located is 1 mm; the thickness of the substrate with an air cavity is 2 mm; and the thickness of the bottom substrate with ground is 0.508 mm. Vertical interconnect accesses (VIAs) provide connections to all metal layers

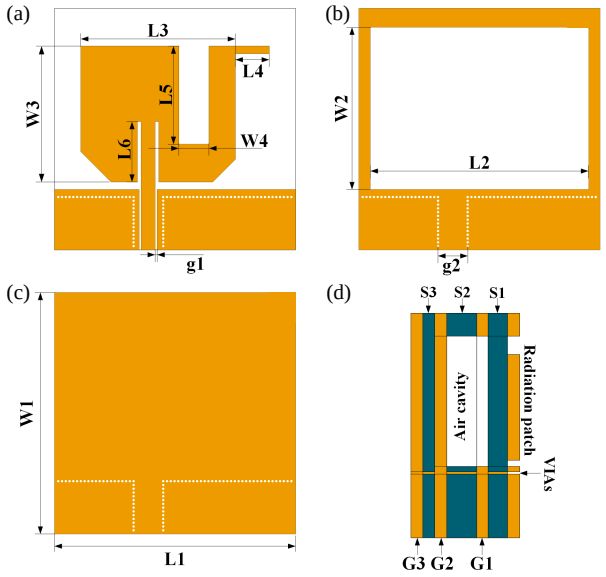

FIGURE 1. Configurations of the antenna (unit: mm). (a) Top view. (b) Ground $G1$ with a cutout. (c) Bottom ground $G2$. (d) Cross-section view.

The radiation patch is situated on a dielectric substrate, $S1$, with its corresponding ground plane, $G1$, shown in Fig. 1(b), followed by a second substrate, $S2$, and its ground plane, $G2$, as depicted in Fig. 1(c). $G1$ and $S2$ have the same cutout region, and together with the remaining parts of $G2$ and $S1$, they form an air cavity positioned directly under the radiation patch. The specific dimensions are detailed in Table 1, including the overall length and width ($L1$ and $W1$), dimensions of the etched sections ($L2$ and $W2$), and the size of the radiation patch ($L3$ and $W3$). Additionally, $L4$ indicates the length of a segment on the radiation patch, while $W4$ and $L5$ represent the width and length of the notched section, respectively. The feedline's position on the radiation patch is denoted by $L6$. Each VIA has a radius of 0.15 mm, with a center-to-center spacing of 0.5 mm between adjacent VIAs. The distance from the feed line to the edge of the metallic patch is $g1$, and the spacing between VIAs on both sides of the feedline is $g2$. The gap between the radiation patch and feed line is 0.5 mm.

As depicted in Fig. 2(a), the proposed antenna is designed to operate at dual frequency bands, targeting both the X-band and Ku-band. The X-band demonstrates an ultra-wideband (UWB) performance, with a simulated -10 dB bandwidth extending from 7.83 to 12.35 GHz, corresponding to a fractional bandwidth of 44.79%. In contrast, the Ku-band is simulated to function from 12.98 to 14.05 GHz, resulting in a fractional bandwidth of 7.91%. Fig. 2(b) depicts the surface current distribution on the radiation patch of the antenna. By creating slots and additional branches on the radiation patch's surface and by placing the feed line in a non-central position on one side of the radiating patch, the effective path length of the current is increased without expanding the area of the radiation patch, thereby achieving miniaturization of the antenna.

Figures 3(a) to (d) display the radiation patterns at frequencies of 9 GHz, 10 GHz, 11 GHz, and 13.5 GHz, respectively. It is evident that the antenna maintains a directional radiation pattern across these frequencies, with gains of 6.38 dBi, 5.52 dBi, 5.76 dBi, and 3.8 dBi at the respective frequency points. Cross-polarization levels typically exhibit significantly lower levels than their co-polarization counterparts. As shown in Fig. 3, the rotation of the radiation pattern at different frequencies is the result of the combined effect of the antenna's back-cavity reflector structure, asymmetric feeding design, and multi-band operation characteristics. The back cavity forms an equivalent reflector through the metal ground plane. As the frequency changes, the electromagnetic resonance of this structure and the current distribution on the patch surface also change. Combined with the off-center feeding method and the modulation of the current path by the slots, the movement of the strong current radiation region and the displacement of the phase center at different frequencies cause the main radiation lobe direction to be adjusted regularly.

3. EVOLUTIONS AND DISCUSSIONS

The proposed design evolves from a monopole antenna with a DGS, typically used in creating UWB antennas. As shown in Fig. 4, the evolution begins with the original monopole antenna featuring a defected ground in (a), and it then progresses to the relocation of the defected ground to coexist with the radiation patch in the same plane, forming a CPW structure in (b) to integrate with the back air cavity. Subsequently, the design incorporates a back-defected ground $G1$ and a substrate $S2$, which,

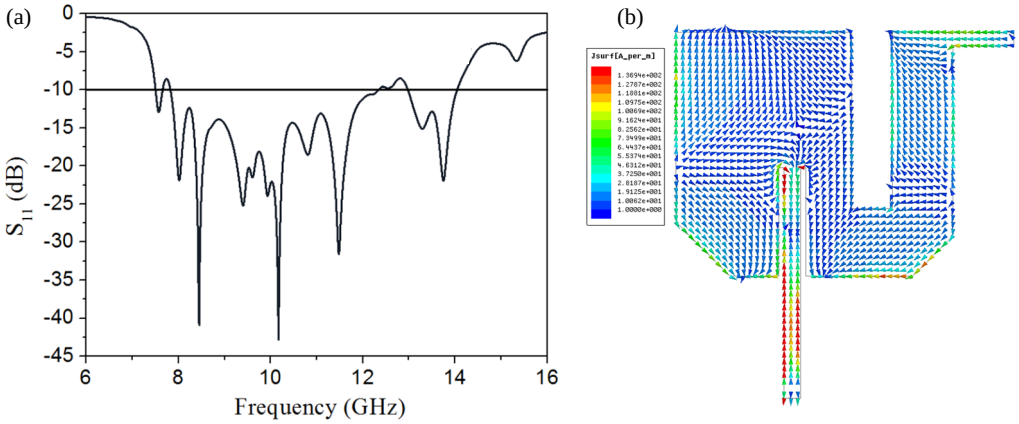

FIGURE 2. S_{11} and the surface current distributions of the antenna. (a) S_{11}. (b) Surface current distribution on the radiation patch.

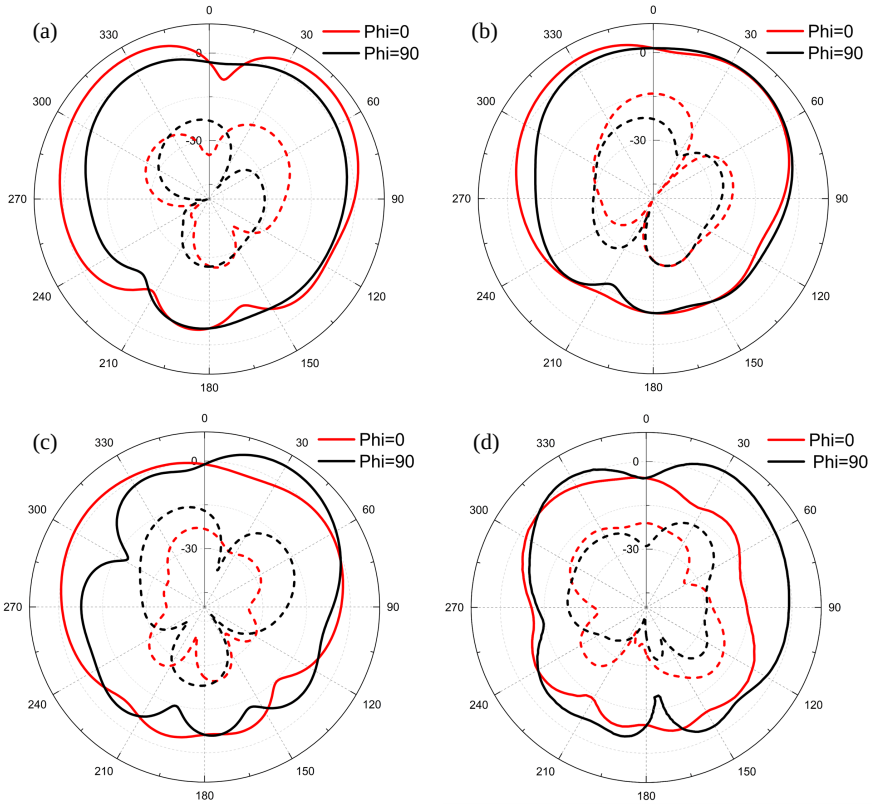

FIGURE 3. Radiation patterns. (a) At 9 GHz. (b) At 10 GHz. (c) At 11 GHz. (d) At 13.5 GHz.

as depicted in Figs. 1(d) and (e), is enclosed by a continuous metallic ground $G2$. This enclosure forms an air cavity directly beneath the radiation patch, creating a resonant structure that eliminates the need for VIAs. The final design, as illustrated in Fig. 1, includes the integration of VIAs to connect all metal layers, as illustrated in Fig. 4(c). A comparison of S-parameters for these evolutionary designs is presented in (d).

As observed in Fig. 4(d), the monopole antenna with a DGS exhibits dual-band operation characteristics, resonating at 8.95 GHz and 11.85 GHz. After transitioning to a CPW structure, the resonant frequencies shift to 9.58 GHz and 11.71 GHz. However, the integration of a back-air cavity introduces three operational bands at 8.25–10.25 GHz, 10.81–12.63 GHz, and 14.04–15.40 GHz. The proximity of the first and second bands prompted the strategic placement of VIAs connecting all metal layers on both sides of the feed line and near the radiation patch side of the CPW, effectively merging the first two bands into a broader operational range, as realized in the final dual-band antenna design targeting the X and Ku bands. The peak gain of the original DGS structure in the 8.3–12.4 GHz frequency

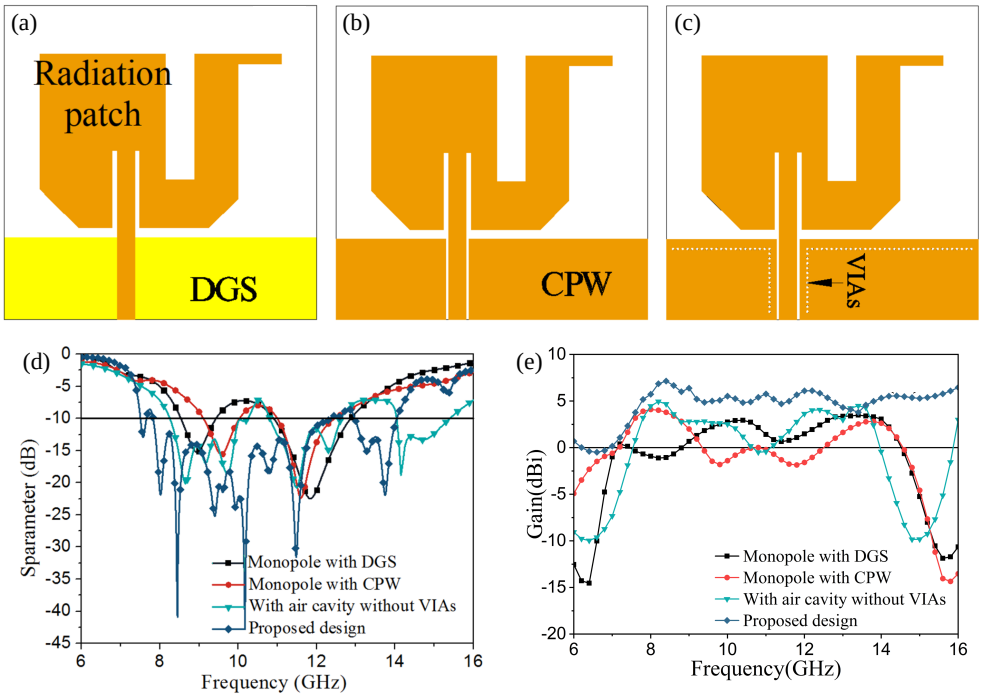

FIGURE 4. Evolutions of the antenna. (a) Monopole with DGS. (b) Monopole with CPW. (c) CPW with VIAs. (d) Comparison of S-parameters. (e) Comparison of Gain Curves at Different Frequencies.

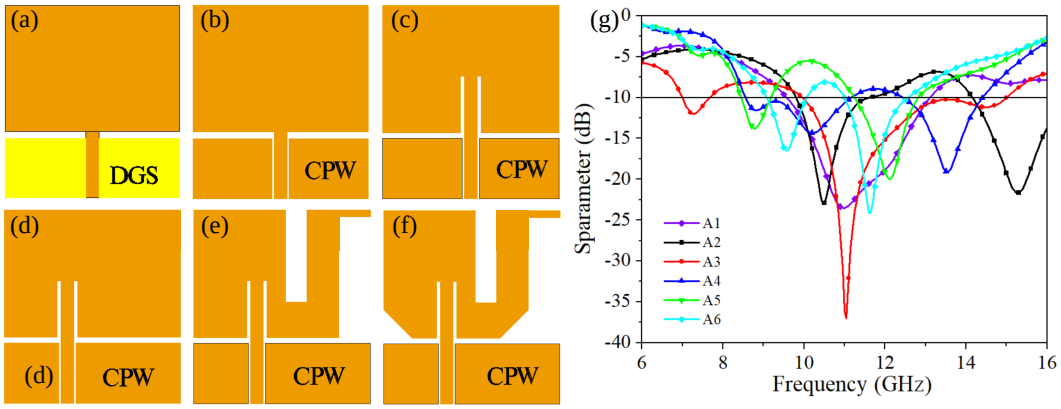

FIGURE 5. Evolutions of the patch. (a) Monopole with DGS. (b) Monopole with CPW. (c) Monopole with CPW and match slots. (d) Asymmetric feed. (e) With slots on patch. (f) With chamfer cuts. (g) S-parameters.

band is 3 dBi. After it is transformed into the CPW structure, the peak gain becomes 4.1 dBi, with a gain increase of 36.67%. Then, when transforming from the CPW structure to the back-cavity structure without vias, the peak gain in the 8.3–14.6 GHz frequency band is 4.95 dBi, with a gain increase of 20.73%. Finally, when transforming from the back-cavity structure without vias to the proposed multi-layer back-cavity via structure, the peak gain in the 8.3–14.21 GHz frequency band is 7.13 dBi, with a gain increase of 44%.

Figure 5 further elucidates the evolutionary development of the antenna patch, labeling the patches from (a) to (f) as A1 through A6. Their corresponding S_{11} parameters are depicted in Fig. 5(g). As previously mentioned, monopole A1, equipped with a DGS, demonstrates a wide-band capability. The antenna exhibits dual-band characteristics when the DGS is modified to a CPW configuration in A2. Incorporating impedance-matching slots adjacent to the feed line on both sides of the patch enhances port impedance matching, transforming the dual-band of A2 into the broad bandwidth of A3. Transitioning the feed line to an asymmetric structure in A4 lowers its resonant frequency. Based on A4, the removal of a $4 \times 13\,\text{mm}^2$ slot and a $4.5 \times 17\,\text{mm}^2$ slot from the patch reduces the patch area of A5 by 28.55%, shifting the corresponding resonance point downward. A6 further refines the design by excavating two chamfer cuts, reducing the patch area by an additional 3.55%, which results in an increase in the low-frequency resonance point and a decrease in the high-frequency resonance point.

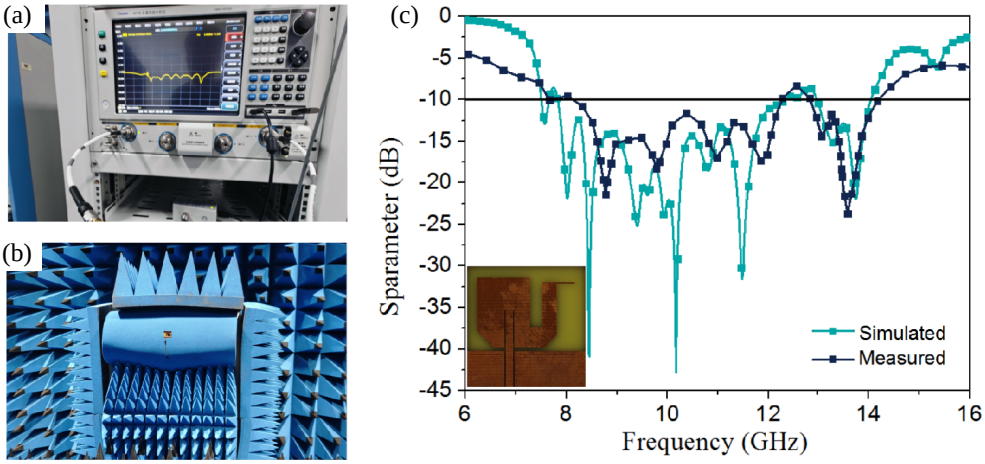

FIGURE 6. Measurement setup and results. (a) and (b) Setup of the measurement. (c) S-parameters.

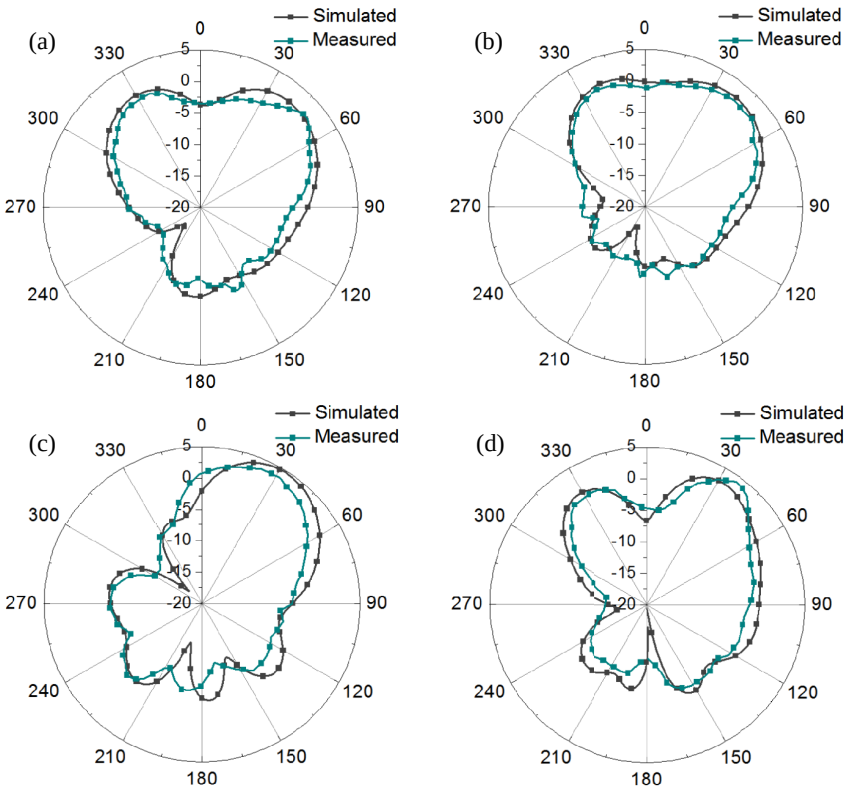

FIGURE 7. Comparison of the measured and simulated radiation patterns. (a) At 9 GHz. (b) At 10 GHz. (c) At 11 GHz. (d) At 13.5 GHz.

4. MEASUREMENT AND COMPARISON

The antenna prototype was fabricated and subsequently measured, with the measurement setup depicted in Fig. 6(a). The antenna measurement process was conducted using a Ceyear Vector Network Analyzer (VNA) model 3672B (10 MHz–26.5 GHz). The analyzer solved the error terms in the error model by measuring high-quality calibration standards (e.g., open, short, load, and thru devices), thereby eliminating systematic errors prior to measurement. The antenna employed SMA-KE connectors with a characteristic impedance of 50 Ω and a frequency range of DC-18 GHz. A comparison of the measured and simulated S-parameters, and the radiation pattern at $\phi = 0°$ are presented in Fig. 6(c) and Fig. 7, respectively. As observed in Fig. 6(c), the antenna operates over the frequency ranges of 8.30–12.29 GHz (38.75% fractional bandwidth) and 12.91–14.21 GHz (9.58% fractional bandwidth). There is a minor deviation in the operating frequency bands compared to the simulated results, with the X-band showing a reduced bandwidth and the Ku-band exhibiting an expanded range. Due to the poor high-frequency performance of the FR4 substrate, certain discrepancies exist between the simulation

TABLE 2. Comparison with other designs.

Ref.	Freq. (GHz)	BW (%)	Peak gain (dBi)	Size (λ_0)
[3]	7.18–8.02, 11.55–12.44	11.05, 7.41	8.07	0.16 (C-band), 0.41 (Ku-band)
[18]	9.71–11.41	15.92	5.71	1.09
[19]	10, 15.2, 17.65	/, /, 1.7	6.3	0.43 (10 GHz)
[20]	3–11.2	116	5	0.48 (8 GHz)
[21]	2.9–14.2	132	5.1	0.51 (8.5 GHz)
This work	8.30–12.29, 12.91–14.21	38.75 (X-band), 9.58 (Ku-band)	7.13	0.53 (X-band), 0.92 (Ku-band)

and measurement results. For operating frequencies below 8 GHz, the figures demonstrate excellent agreement between the simulated and measured results. However, when the frequency exceeds 8 GHz, observable deviations emerge. These discrepancies primarily arise from the increased dielectric loss and reduced permittivity of the FR4 substrate at frequencies above 8 GHz, which elevate the antenna's resonant frequency and result in a slight reduction in bandwidth. Fig. 7 illustrates that the antenna's simulated and measured radiation patterns at multiple frequency points are in close agreement with the patterns being measured in an anechoic chamber.

Table 2 compares the proposed antenna against existing designs, revealing its distinct advantages in multi-band functionality and compactness (λ_0 is the wavelength of the center frequency in the free space). This comparison underscores the superior attributes of our design.

5. CONCLUSIONS

This paper presents the design and evolution of a novel dual-band CPW antenna with an integrated back cavity for directional radiation. The antenna's innovative design transitions the DGS structure to a CPW feeding mechanism, strategically positions VIAs along the feed line and near the CPW radiation patch, integrates the radiation patch with an air cavity behind it, and significantly reduces the radiation patch area by 32.11% through asymmetric feeding and loading slits and chamfer cuts on the patch. The result is a compact, high-performance integrated antenna. Simulation and measurement results show that the antenna covers the frequency ranges of 8.30–12.29 GHz (38.75% fractional bandwidth) and 12.91–14.21 GHz (9.58% fractional bandwidth). The agreement between the measured and simulated results substantiates the precision of the design and confirms efficient operation within the targeted frequency bands. Moreover, the current design has already enabled the antenna to operate in dual bands, namely the X and Ku bands. However, there is still room for improvement. Future research will mainly focus on two aspects: first, expanding the bandwidth, increasing the number of frequency bands, and enhancing the radiation efficiency. The methods to achieve bandwidth expansion or add more frequency bands include: optimizing the shape of the radiating patch, adjusting the antenna's resonant frequency and bandwidth by changing its shape, adjusting the dimensions of the Defected Ground Structure (DGS), controlling the antenna's operating bandwidth by taking advantage of its influence on the electromagnetic field distribution, exploring new substrate materials, and improving the antenna's performance by virtue of their characteristics such as low dielectric loss and high permittivity. Second, improving radiation efficiency can be achieved by optimizing the back-cavity structure (for example, by adjusting the depth and shape of the air cavity) to reduce energy dissipation and guide the radiation more efficiently.

In addition, integrating the antenna into an array configuration is also a promising direction. The combination of multiple antennas in an array can enhance the antenna's directivity and gain, which is beneficial for applications such as satellite communication and radar systems that require high-performance antennas. In conclusion, the antenna's compact design, wide bandwidth, and appropriate gain make it suitable for modern wireless communication systems. Future research focusing on bandwidth and frequency band expansion, radiation efficiency enhancement, and antenna array integration will further optimize its performance and expand its application fields.

ACKNOWLEDGEMENT

This work was supported by "the Fundamental Research Funds for the Central Universities", Southwest Minzu University (ZYN2024134).

REFERENCES

[1] Sun, F., X. Wu, N. Ou, Y. Luan, and W. Yu, "A dual-band X/Ku co-polarized shared-aperture waveguide slot antenna," *IEEE Antennas and Wireless Propagation Letters*, Vol. 23, No. 12, 4418–4422, 2024.

[2] Su, T., X. Yi, and B. Wu, "X/Ku dual-band single-layer reflectarray antenna," *IEEE Antennas and Wireless Propagation Letters*, Vol. 18, No. 2, 338–342, 2019.

[3] Zahid, M., M. M. Taqdeer, and Y. Amin, "A compact dual-band microstrip patch antenna for C-and X-and Ku-band applications," *Engineering Proceedings*, Vol. 46, No. 1, 16, 2023.

[4] Derafshi, I., N. Komjani, E. Ghasemi-Mizuji, and M. Mohammadirad, "Dual-band X/Ku reflectarray antenna using a novel FSS-backed unit-cell with quasi-spiral phase delay line," *Journal of Microwaves, Optoelectronics and Electromagnetic Applications*, Vol. 15, No. 3, 225–236, 2016.

[5] Deng, R., S. Xu, F. Yang, and M. Li, "Design of a low-cost single-layer X/Ku dual-band metal-only reflectarray antenna," *IEEE Antennas and Wireless Propagation Letters*, Vol. 16, 2106–2109, 2017.

[6] Acharya, P., J. Kumar, and V. Dahiya, "A novel violin type UWB patch antenna for X & Ku bands using metamaterial: A review," in *2022 2nd International Conference on Artificial Intelligence and Signal Processing (AISP)*, 1–6, Vijayawada, India, 2022.

[7] Wang, H., L. Chang, Y. Li, K. Wei, and Z. Zhang, "A deployable coplanar waveguide CoCo antenna," *IEEE Antennas and Wireless Propagation Letters*, Vol. 23, No. 10, 3083–3087, 2024.

[8] Hu, D., X. Liang, L. Zhang, S. Li, W. Cheng, F. Kong, and Q. Tan, "Coplanar waveguide antenna for surface acoustic wave temperature-pressure dual sensors," *IEEE Sensors Journal*, Vol. 24, No. 9, 14 962–14 969, 2024.

[9] Agustina, S., A. Athiroh, N. F. A. Hakim, and I. Kustiawan, "Coplanar waveguide antenna using resistive load for wireless communication systems," in *2021 3rd International Symposium on Material and Electrical Engineering Conference (ISMEE)*, 217–221, Bandung, Indonesia, Nov. 2021.

[10] Yang, Q., S. Gao, Q. Luo, L. Wen, Y.-L. Ban, X.-X. Yang, X. Ren, and J. Wu, "Cavity-backed slot-coupled patch antenna array with dual slant polarization for millimeter-wave base station applications," *IEEE Transactions on Antennas and Propagation*, Vol. 69, No. 3, 1404–1413, 2021.

[11] Mukherjee, S., A. Biswas, and K. V. Srivastava, "Substrate integrated waveguide cavity backed slot antenna with parasitic slots for dual-frequency and broadband application," in *2015 9th European Conference on Antennas and Propagation (EuCAP)*, 1–5, Lisbon, Portugal, 2015.

[12] Chen, R.-S., L. Zhu, J.-Y. Lin, S.-W. Wong, Y. Yang, Y. Li, L. Zhang, and Y. He, "High-isolation in-band full-duplex cavity-backed slot antennas in a single resonant cavity," *IEEE Transactions on Antennas and Propagation*, Vol. 69, No. 11, 7092–7102, 2021.

[13] Yi, D., L. Tang, L.-P. Feng, L.-L. Qian, Z.-Y. Qi, M.-C. Tang, X.-C. Wei, and E.-P. Li, "Compact, co-polarized, and in-band filtering cavity-backed slot-antenna pair based on multifunctional metasurface diaphragms," *IEEE Transactions on Antennas and Propagation*, Vol. 72, No. 4, 3250–3261, 2024.

[14] Dai, H.-N., K.-W. Ng, M. Li, and M.-Y. Wu, "An overview of using directional antennas in wireless networks," *International Journal of Communication Systems*, Vol. 26, No. 4, 413–448, 2013.

[15] George, R. and T. A. J. Mary, "Review on directional antenna for wireless sensor network applications," *IET Communications*, Vol. 14, No. 5, 715–722, 2020.

[16] Kumar, A. and D. K. Singh, "A review with new approaches of reflector antenna," in *2020 International Conference on Advances in Computing, Communication & Materials (ICACCM)*, 162–167, Dehradun, India, 2020.

[17] Zha, S., Z. Qu, J. Zhang, D. Zheng, and P. Liu, "A gain reconfigurable reflector antenna with surface mounted field-induced artificial magnetic conductor for adaptive HIRF prevention," *IEEE Transactions on Antennas and Propagation*, Vol. 72, No. 9, 7252–7260, 2024.

[18] Althuwayb, A. A., D. Chaturvedi, and A. Kumar, "Substrate integrated waveguide (SIW) cavity-backed slot antenna with monopole-like radiation for vehicular communications," *Applied Physics A*, Vol. 128, No. 3, 202, 2022.

[19] Taha İmeci, Ş., B. Tütüncü, and L. Herceg, "Performance-enhanced S-shaped slotted patch antenna for X band/Ku band applications," *Wireless Personal Communications*, Vol. 129, No. 2, 1069–1082, 2023.

[20] Abdollahvand, M., B. A. Arand, K. Katoch, and S. Ghosh, "A novel and compact ultra-wideband printed monopole antenna with enhanced bandwidth and dual-band stop properties," *Microwave and Optical Technology Letters*, Vol. 66, No. 1, e33990, 2024.

[21] Abdollahvand, M., Y. Zehforoosh, B. Marufi, P. E. Kaleybar, and A. Dastranj, "A novel UWB in-body printed microstrip feed monopole antenna with dual band-stop capabilities," *Microwave and Optical Technology Letters*, Vol. 66, No. 9, e34317, 2024.